ACS Catalysis

Research Article

pubs.acs.org/acscatalysis

Mechanistic Insights on the Hydrogenation of α,β-Unsaturated Ketones and Aldehydes to Unsaturated Alcohols over Metal Catalysts

Matthew S. Ide,[†] Bing Hao,[†] Matthew Neurock,[†,‡] and Robert J. Davis*[,†]

Departments of [†]Chemical Engineering and [‡]Chemistry, University of Virginia, 102 Engineers' Way, PO Box 400741, Charlottesville, Virginia 22904-4741, United States

Supporting Information

ABSTRACT: The selective hydrogenation of unsaturated ketones (methyl vinyl ketone and benzalacetone) and unsaturated aldehydes (crotonaldehyde and cinnamaldehyde) was carried out with H_2 at 2 bar absolute over Pd/C, Pt/C, Ru/C, Au/C, Au/TiO_2, or Au/Fe_2O_3 catalysts in ethanol or water solvent at 333 K. Comparison of the turnover frequencies revealed Pd/C to be the most active hydrogenation catalyst, but the catalyst failed to produce unsaturated alcohols, indicating hydrogenation of the C═C bond was highly preferred over the C═O bond on Pd. The Pt and Ru catalysts were able to produce unsaturated alcohols from unsaturated aldehydes, but not from unsaturated ketones. Although Au/Fe_2O_3 was able to partially hydrogenate unsaturated ketones to unsaturated alcohols, the overall hydrogenation rate over gold was the lowest of all of the metals examined. First-principles density functional theory calculations were therefore used to explore the reactivity trends of methyl vinyl ketone (MVK) and benzalacetone (BA) hydrogenation over model Pt(111) and Ru(0001) surfaces. The observed selectivity over these metals is likely controlled by the significantly higher activation barriers to hydrogenate the C═O bond compared with those required to hydrogenate the C═C bond. Both the unsaturated alcohol and the saturated ketone, which are the primary reaction products, are strongly bound to Ru and can react further to the saturated alcohol. The lower calculated barriers for the hydrogenation steps over Pt compared with Ru account for the higher observed turnover frequencies for the hydrogenation of MVK and BA over Pt. The presence of a phenyl substituent α to the C═C bond in BA increased the barrier for C═C hydrogenation over those associated with the C═C bond in MVK; however, the increase in barriers with phenyl substitution was not adequate to reverse the selectivity trend.

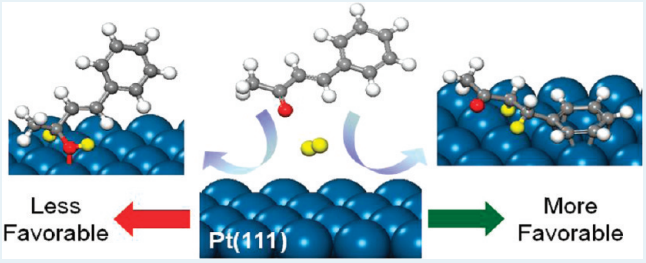

KEYWORDS: *α,β-unsaturated ketones, α,β-unsaturated aldehydes, selective hydrogenation, density functional theory, ruthenium, platinum, palladium, gold*

INTRODUCTION

The selective hydrogenation of α,β-unsaturated ketones and aldehydes to unsaturated alcohols is a critical step in the synthesis of chemical intermediates used in the production of pharmaceuticals, cosmetics, and foods.[1] These reactions are often carried out in batch processes using homogeneous catalysts[2,3] or in hydrogen transfer solvents.[4−6] The development of heterogeneous catalytic materials to carry out these conversions would significantly improve process efficiency as well as process economics. However, several challenges arise in the selective hydrogenation of α,β-unsaturated carbonyl compounds. The addition of hydrogen to the conjugated C═C bond is both thermodynamically and kinetically favored over the C═O bond.[7] Nevertheless, α,β-unsaturated ketones and aldehydes can sometimes be selectively hydrogenated to the unsaturated alcohols, provided the reactions are run over certain catalysts at sufficiently low temperature and pressure.

The steric hindrance associated with bulky substituent groups near the C═C bond is also thought to play an important role in determining selectivity, such as for ketones present in ring structures.[8,9] Steric hindrance near the C═C bond cannot alone explain why there is a lack of selectivity to the unsaturated alcohol for most α,β-unsaturated ketone hydrogenation reactions over Pd, Pt, and Ru catalysts,[10−12] since these metals can sometimes selectively hydrogenate α,β-unsaturated aldehydes with similar sterically hindered C═C bonds. In this work, a systematic experimental study of the effect of metal type, support composition, and reactant structure on the catalytic activity and product selectivity is combined with density functional theory (DFT) quantum chemical calculations to elucidate the critical factors that control selectivity during the hydrogenation of α,β-unsaturated ketones to unsaturated alcohols.

Palladium, platinum, and ruthenium have been tested extensively in the hydrogenation of α,β-unsaturated aldehydes.[13] Palladium appears to be the most selective in forming saturated aldehydes,[14−16] and ruthenium[15−20] and platinum[21−24] are moderately selective toward the formation of the unsaturated

Received: November 2, 2011
Revised: March 12, 2012
Published: March 14, 2012

alcohols. The degree of substitution in α,β-unsaturated aldehydes has also been shown to greatly affect selectivity. Galvagno et al. observed the selectivity to the unsaturated alcohol was greater for citral than cinnamaldehyde over Ru/C catalysts that ranged in particle size from 2 to 12 nm.[17,18] These results were supported by the work of Mercadante et al. with particles below 8 nm; however, increasing the Ru particle size from 8 to 27 nm on both Ru/C and Ru/Al_2O_3 increased selectivity to the unsaturated alcohol during cinnamaldehyde hydrogenation, whereas no effect on selectivity during citral hydrogenation was observed.[19] Several different Pt/Al_2O_3 catalysts exhibited higher selectivity to the unsaturated alcohol product from cinnamaldehyde than from either 3-methylcrotonaldehyde or crotonaldehyde,[23] and the selectivity difference was significant, regardless of the catalyst reduction temperature.

In addition to the type of metal and the presence of substituent groups on the reactant molecule, the composition of the support and the presence of promoters can also influence hydrogenation performance. For example, Mercadante et al. showed that a Ru/C catalyst was ∼20% more selective to the unsaturated alcohol than a Ru/Al_2O_3 catalyst for cinnamaldehyde hydrogenation.[19] Moreover, Lashdaf et al. observed a higher selectivity during cinnamaldehyde hydrogenation over Ru/SiO_2 compared with Ru/Al_2O_3.[15] The increased selectivity to unsaturated alcohol (UA) during crotonaldehyde hydrogenation over a Pt/TiO_2 catalyst reduced at 773 K compared with 573 K was explained by the increased reduction of metal oxide species during the high temperature reduction.[22] The literature also indicates that although Pt and Ru catalysts containing Sn promoters are effective at selectively hydrogenating unsaturated aldehydes to unsaturated alcohols,[12,25−28] they are not selective in hydrogenating simple unsaturated ketones, such as methyl vinyl ketone (MVK), to the unsaturated alcohol.[12] A more complete discussion on the effects of promoters on aldehyde and ketone hydrogenation can be found in the review by Ponec.[29]

The selective hydrogenation of α,β-unsaturated aldehydes[30−37] and ketones[11,30,38−40] over supported gold catalysts has been demonstrated recently, even though the exact role of gold in the reaction is still under debate. Interestingly, Au/Fe_2O_3 has catalyzed the selective hydrogenation of benzalacetone (BA) to the unsaturated alcohol.[40] Goethite (crystalline iron oxide) was the preferred structure of the support for Au particles compared with maghemite and hematite.[39] The surface area of the iron oxide support and the size of the gold metal particles did not appear to affect the selectivity of the reaction. Although the first-order rate constant for BA hydrogenation over Au/Fe_2O_3 was higher than that for cinnamaldehyde on the same catalyst,[30] the selective hydrogenation of α,β-unsaturated aldehydes over supported Au generally follows the same trends as α,β-unsaturated ketones.[35] However, the gold particle size has been directly correlated to the selectivity to unsaturated alcohols for α,β-unsaturated aldehydes over Au/ZnO, Au/ZrO_2, Au/TiO_2, and Au/SiO_2, with larger particles being more selective.[33,36,37] In contrast, the selectivity during acrolein hydrogenation was reported to be independent of gold particle size over Au/TiO_2.[34]

Previous theoretical studies reported in the literature examined the adsorption[41−44] and hydrogenation[45−51] of acrolein and other unsaturated aldehydes over model Pt(111)[42,45] and Ag(110)[46] surfaces as well as over alloyed surfaces ($Pt_{80}Fe_{20}$[47,48]). These studies show that the adsorption of acrolein on Pt(111) occurs predominantly via a di-σ interaction in which the C═C bond is rehybridized to form two M-C σ-bonds with the surface. The oxygen atom of the carbonyl only weakly interacts with the metal surface.[41,42,52] Substituents on the C═C bond, such as those found in crotonaldehyde and prenal, destabilize the interactions between the aldehyde and the metal surface. This destabilization helped to explain the selectivity patterns during hydrogenation reactions over model transition metal surfaces.[41] The presence of iron atoms in the surface layer of $Pt_{80}Fe_{20}$ alloy was found to enhance the selectivity toward unsaturated alcohol because Fe increases the interaction between the C═O group and the surface.[47,48]

Surface coverage of adsorbed species can also change the adsorption mode,[42,49] as has been observed for acrolein, crotonaldehyde, and prenal on Pt(111).[41] The results for the selective hydrogenation of acrolein over Pt(111) indicate that it is actually easier to hydrogenate the C═O bond than the C═C bond[45] and that the low selectivity to allyl alcohol is due to its hindered desorption from the surface.[45,50] In contrast to Pt(111), selective hydrogenation of acrolein on Ag(110) produces allyl alcohol and propanal, which are predicted to desorb more easily from Ag(110).[46] These studies provide important insights into the influence of reactant structures on the hydrogenation of unsaturated aldehydes. In particular, the branching or substitution of bulkier hydrocarbon groups near the C═C bond inhibits its interaction with the surface[41] and favors the selectivity to unsaturated alcohols.[51] Despite the extensive studies on unsaturated aldehydes, there are very few, if any, detailed theoretical studies reported on the hydrogenation of unsaturated ketones.

Given the widely varying studies of selective hydrogenation over precious metals on different supports under various reaction conditions, a systematic exploration of selective hydrogenation reactions under well controlled experimental conditions and by quantum chemical methods would help to establish the factors that control the reactivity and selectivity for these reactions. Thus, the present study examines carbon-supported Pd, Pt, Ru, and Au catalysts for the hydrogenation of MVK and crotonaldehyde in aqueous solution as well as BA and cinnamaldehyde in ethanol solvent to explore the role of metal type and reactant structure on the activity and selectivity trends associated with α,β-unsaturated ketones and aldehydes. To determine the effect of the support on these reactions, Au/C, Au/TiO_2, and Au/Fe_2O_3 were also evaluated as hydrogenation catalysts. First principles periodic density functional theoretical calculations[53] were carried out to examine the reaction mechanism and to provide insights into the factors that control selectivity during MVK and BA hydrogenation on model Pt and Ru surfaces.

EXPERIMENTAL METHODS

Catalysts. Carbon-supported Pd and Ru catalysts were obtained from Acros Organics, and a carbon-supported Pt catalyst was obtained from Sigma-Aldrich. The 5 wt % Ru/C (50% w/w water) was dried in air at 433 K overnight before use. The 2.9 wt % Pd/C and 3.0 wt % Pt/C were used as received.

Gold catalysts were obtained from the World Gold Council. A 0.8 wt % Au on carbon (type C, sample 40D) catalyst, a 1.6 wt % Au/TiO_2 catalyst (no. 52A, Lot. No. 02-05) and a 4.4 wt % Au on Fe_2O_3 catalyst (type 64C, Lot. No. 02-05) were used in this study.

dx.doi.org/10.1021/cs200567z | ACS Catal. 2012, 2, 671−683

Chemisorption of H_2. The metal dispersion of the Pd/C, Pt/C, and Ru/C catalysts was determined by H_2 chemisorption using a Micromeritics ASAP 2020 automated adsorption analyzer. The Pd/C catalyst was heated to 473 K at a rate of 4 K/min under flowing H_2 (GT&S 99.999%). The sample was evacuated and held for 2 h at 473 K before being cooled to 373 K for analysis. The analysis was carried out at 373 K in the pressure range of 40−450 Torr to avoid formation of the β-phase hydride. The Ru/C and Pt/C catalysts were heated to 523 at 4 K/min under flowing H_2 (GT&S 99.999%). The samples were evacuated and held for 2 h at 523 K before being cooled to 308 K for analysis in the pressure range of 40−450 Torr. The amount of metal on the surface was evaluated by the total amount of H_2 adsorbed extrapolated to zero pressure, assuming a stoichiometry (H/M_{surf}, M = Ru, Pd, and Pt) equal to unity.

Hydrogenation Reactions. The hydrogenation of methyl vinyl ketone (Sigma Aldrich, 99%), crotonaldehyde (Sigma Aldrich, 99%), benzalacetone (Sigma Aldrich, 99%), and cinnamaldehyde (Sigma Aldrich, 99%) was conducted in a 100 cm^3 stainless steel Parr Instruments Company 4565 batch reactor equipped with an electronic temperature controller, a mechanical stirrer, a dip tube for sampling, and a glass liner. Distilled, deionized water was used as an environmentally benign solvent in methyl vinyl ketone and crotonaldehyde hydrogenation. Ethanol (Sigma Aldrich, 99.5%) was used as a solvent in benzalacetone and cinnamaldehyde hydrogenation because both compounds are only slightly soluble in water.

In all reactions, 25 cm^3 of solvent was added to the reactor along with an appropriate amount of catalyst. The reactor was pressurized to 2 atm absolute and heated to 333 K with flowing H_2 (GT&S 99.999%). The catalyst was then reduced for 2 h by flowing H_2 (2 atm absolute) at 150 cm min^{-1} at 333 K while stirring at 700 rpm. The substrate was added to start the reaction. Liquid samples were allowed to cool to room temperature before analysis. The reactor was backfilled with H_2 after each sample to maintain a constant pressure of 2 atm absolute. The catalyst was removed from a sample by filtration using a 0.2 μm syringe filter (Fisher).

Liquid samples were analyzed by gas chromatography (GC) using an Agilent 7890A GC equipped with an FID detector. The GC utilized an Agilent DB-Wax column of size 30 m × 0.53 mm i.d. × 1 μm. The retention times and response factors for the observed products were determined by injecting known concentrations with an internal standard. The absence of external mass-transfer limitations was determined by varying the catalyst amount and stirring rate. External mass transfer limitations were negligible over Pd/C (the most active catalyst) at a substrate/surface metal ratio above 3500 and a stirring speed of 700 rpm. Therefore, a molar ratio of ~5000 substrate molecules to surface metal atoms was used for all runs. The initial concentration of the substrate was kept constant at 0.2 M, except where noted.

Conversion of MVK in aqueous solution was not observed after typical reaction times over Pd/C and Ru/C when N_2 was substituted for H_2. Moreover, the total MVK conversion after 24 h with no catalyst in the reactor was 0.3%. The total carbon balance typically closed to within 10%.

DFT Calculations. First principles DFT calculations were carried out to determine the adsorption energies for all reactants, intermediates and products as well as the activation barriers and reaction energies involved in hydrogenating the C═C and C═O bonds of MVK and BA. All of the DFT calculations reported herein were performed using the Vienna ab initio simulation package (VASP).[54] The Perdew−Wang 91 form of the generalized gradient approximation was used to calculate nonlocal gradient corrections to the correlation and exchange energies.[55] The wave functions were constructed from the expansion of planewaves with an energy cutoff of 396 eV. The electron−ion interactions in the core region were described by Vanderbilt ultrasoft pseudopotentials with real space projection operators.[56] The energies of the absorbates in vacuum were calculated spin-polarized using a 16 × 16 × 16 Å unit cell. All of the calculations involving the nonmagnetic ruthenium and platinum metal surfaces were performed non-spin-polarized. The geometry optimizations were carried out via a three-step process, in which the first step converged the atomic structures to a point where the forces on all of the atoms were less than 0.10 eV/Å, followed by a second optimization step to reduce the forces to 0.05 eV/Å with the wave functions converged to 1×10^{-6} eV. Both the first and second steps were performed using 3 × 3 × 1 Monkhorst−Pack k-point mesh to sample the Brillouin zone integration,[57,58] whereas the final step was carried out using a 6 × 6 × 1 k-point mesh to determine the lowest energy structure. A 6 × 6 × 1 k-point mesh was used in the third and final step to ensure a higher level of accuracy on the electronic energy. These calculations were carried out as static single-point calculations. Structural optimizations carried out at a tighter convergence of 0.01 eV/Å on the forces led to changes in the energy of less than 1 kJ mol^{-1}. As such, we did not increase the convergence on the forces beyond the 0.05 eV/Å.

The bulk lattice constants for Pt and Ru were initially set to the experimental values of a = 3.92 Å for Pt and a = 2.71 Å for Ru and then optimized within VASP. The optimized values of a = 3.99 and 2.70 Å were subsequently used in the construction of the Pt(111) and Ru(0001) surfaces.[59,60] Metal surfaces were modeled using a 4 × 4 unit cell to accommodate the reacting species and minimize spurious cell-to-cell interactions with four metal layers, and a 16 Å vacuum region to separate the slabs in the z-direction. The top two metal layers were allowed to relax, while the bottom two layers were fixed to their optimized bulk lattice positions. Adsorption was examined only at the top surface of the slab. The adsorption energies were calculated as $\Delta E_{ads} = E_{metal+adsorbate} - E_{adsorbate} - E_{metal}$, where a negative value indicates that the adsorption is exothermic.

The transition state, or saddle point on the minimum energy path (MEP), was located through combining the nudged elastic band (NEB) method[61,62] to establish images along the MEP that bracket the transition state and the Dimer method[63,64] to isolate the specific transition state. In the NEB calculations, an initial series of intermediate images were refined using a 3 × 3 × 1 k-point mesh until the maximum force on each atom decreased to 0.20 eV/Å. Dimer calculations were subsequently carried out by 3 × 3 × 1 k-point until the maximum atomic forces converged to 0.05 eV/Å, and finally, a 6 × 6 × 1 k-point was used to determine the energy of the transition state (TS). All of the transition states reported for the hydrogenation of MVK have been confirmed by carrying out vibrational frequency calculations to show that there is only one imaginary frequency corresponding to the reaction path. The transition states for benzalacetone were found to be very similar, and as such, we did not carry out the vibrational frequency analysis. The intrinsic activation barriers and overall reaction energies were determined by calculating the energy difference between the transition state and the reference state (reactant adsorbate

dx.doi.org/10.1021/cs200567z | ACS Catal. 2012, 2, 671−683

and H atom at an infinite distance on the surface) and the product and the reference state, respectfully.

The calculations were carried out using a constant surface coverage of 1/16 species ML (1 adsorbate per unit cell), which is much lower than the saturation coverage to avoid strong repulsive interaction between adsorbates. Higher surface coverage of the unsaturated ketone and hydrogen reactants will result in lateral repulsive interactions, which decrease the calculated activation barriers for hydrogenation reactions.[65] A comparison of the changes in the adsorption energy with coverage is reported in the Supporting Information (Table S1).

Although the experimentally measured hydrogenation rates were evaluated in the presence of a solvent, for the sake of simplicity, all of the DFT calculated reactions reported herein were carried out in vapor phase. Our previous results that were determined in aqueous media over metal surfaces indicate that barriers for hydrogenating oxygenates in the presence of a polar solvent can be decreased by as much as 20 kJ mol^{-1} compared with those determined without a solvent because of a stabilization of the partially charged transition states by the polar solvent.[66,67]

RESULTS AND DISCUSSION

Catalyst Characterization. The results from H_2 chemisorption are reported in Table 1. The fraction of metal exposed, or dispersion, for the Pd/C, Pt/C, and Ru/C catalysts was calculated to be 0.32, 0.40, and 0.43, respectively. The similar dispersions of the Pd, Pt, and Ru catalysts indicate that these metal particles are in the range of 2−3 nm. The mean particle size of the Au catalysts as provided by the World Gold Council (WGC) was used to calculate a dispersion of the metal used for the calculation of turnover frequency. The Au/TiO_2 and Au/Fe_2O_3 catalysts have metal particle sizes similar to the other catalysts, whereas the Au/C catalyst had much larger particles.

Table 1. Physical Characteristics of the Catalysts

catalyst	metal loading (%)	metal dispersion	metal particle size (nm)
Pd/C	2.9[a]	0.32[b]	3.3[c]
Pt/C	3.0[a]	0.40[b]	2.5[c]
Ru/C	5.0[a]	0.43[b]	2.3[c]
Au/C	0.8[d]	0.10[e]	10.5[f]
Au/TiO_2	1.6[d]	0.38[e]	2.6[f]
Au/Fe_2O_3	4.4[d]	0.28[e]	3.6[f]

[a]Determined by ICP analysis performed by Galbraith Laboratories (Knoxville, TN). [b]Determined by H_2 chemisorption. [c]Estimated as the inverse of metal dispersion. [d]From ICP analysis provided by the World Gold Council. [e]Estimated as the inverse of mean metal particle size. [f]From TEM analysis provided by the World Gold Council.

Hydrogenation of Methyl Vinyl Ketone and Crotonaldehyde. The hydrogenation products of the α,β-unsaturated ketones and aldehydes are either unsaturated alcohols (UA) or saturated ketones/aldehydes (SK/SAL) by the hydrogenation of the C═O bond or C═C bond, respectively. The saturated alcohol (SA) is produced by the sequential hydrogenation of either intermediate product, as seen in Scheme 1. The comparison of methyl vinyl ketone (MVK) and crotonaldehyde was chosen to contrast the effect of a methyl substituent on C═O versus C═C bond hydrogenation.

Figure 1 shows a typical reaction profile for MVK hydrogenation over Ru/C at 333 K. The normalized moles of a product are calculated as the moles of a specific product formed divided by the total number of moles of all products formed. The profile illustrates the sequential nature of the reaction as MVK is first hydrogenated to the saturated ketone, which subsequently hydrogenates to form the saturated alcohol. The saturated alcohol was produced only after all MVK was

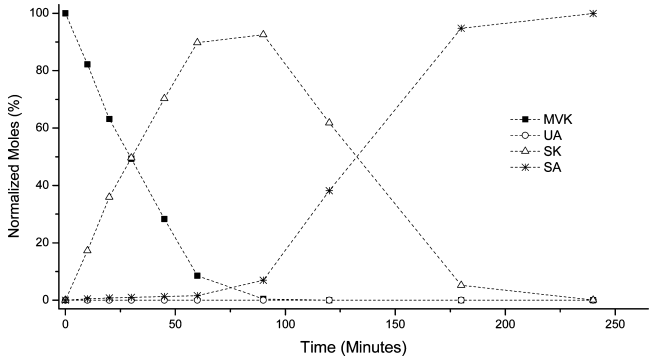

Figure 1. Reaction profile for methyl vinyl ketone (squares, MVK) hydrogenation over Ru/C. The products are saturated ketone (triangles, SK), saturated alcohol (asterisks, SA), and unsaturated alcohol (circles, UA).

Scheme 1. The Reaction Paths for the Hydrogenation of Methyl Vinyl Ketone, Crotonaldehyde, Benzalacetone and Cinnamaldehyde

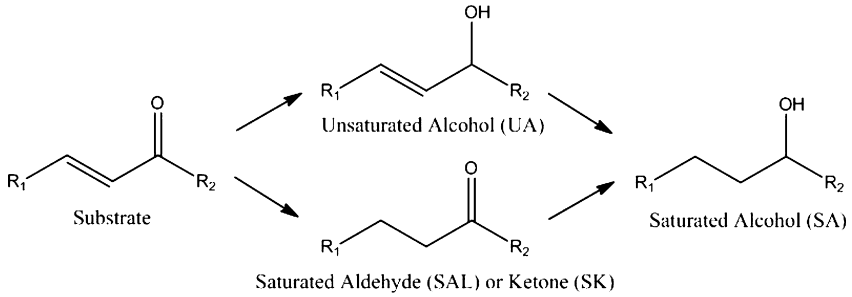

α,β-Unsaturated Ketones	R_1	R_2	α,β-Unsaturated Aldehydes	R_1	R_2
Methyl Vinyl Ketone	H	CH_3	Crotonaldehyde	CH_3	H
Benzalacetone	C_6H_5	CH_3	Cinnamaldehyde	C_6H_5	H

dx.doi.org/10.1021/cs200567z | ACS Catal. 2012, 2, 671−683

converted to saturated ketone. The unsaturated alcohol was not observed under these reaction conditions.

Table 2 summarizes the performance of Ru/C, Pt/C, Pd/C, and Au/C in the hydrogenation of MVK and crotonaldehyde in

Table 2. Hydrogenation of MVK and Crotonaldehyde over Supported Pd, Pt, Ru, and Au Catalysts in Aqueous Solvent[a]

				selectivity (%)[b]		
substrate	catalyst	TOF[c] s^{-1}	conversion (%)[d]	UA	SK/SAL	SA
MVK	Pd/C	2.5	87	0	99	1
MVK	Pt/C	0.94	89	0	98	2
MVK	Ru/C	0.23	72	0	98	2
MVK	Au/C	0.019[e]	26	0	95	5
crotonaldehyde	Pd/C	0.54	92	0	100	0
crotonaldehyde	Pt/C	0.13	68	10	85	5
crotonaldehyde	Ru/C	0.05	61	17	76	7
crotonaldehyde	Au/C	0.015[e]	34	37	52	11

[a]Reaction conditions: 0.2 M substrate, $S/M_{surf} \sim 5000$, $pH_2 = 2$ atm, $T = 333$ K. [b]Selectivity is reported at the level of conversion in the table. [c]Turnover frequency is reported at ~20% conversion. [d]Conversion of MVK or crotonaldehyde. [e]Turnover frequency of Au/C reported at ~10% conversion.

aqueous solvent. The turnover frequency (TOF) was evaluated at ~20% conversion of the substrate over the Ru/C, Pt/C, and Pd/C catalysts and at ~10% conversion of the substrate over Au/C. The TOFs were calculated on the basis of the metal dispersions reported in Table 1. At conversions below 95%, the hydrogenation of MVK over Ru/C, Pt/C, Pd/C, and Au/C formed almost exclusively saturated ketone. This finding is consistent with Marinelli et al., who found 96.6% selectivity toward the saturated ketone in the gas phase over Pt/SiO_2.[10]

If the reagents in the reactor are allowed to continue to react past 100% conversion of MVK, significant amounts of saturated alcohol can form during the reaction. Figure 2 shows the

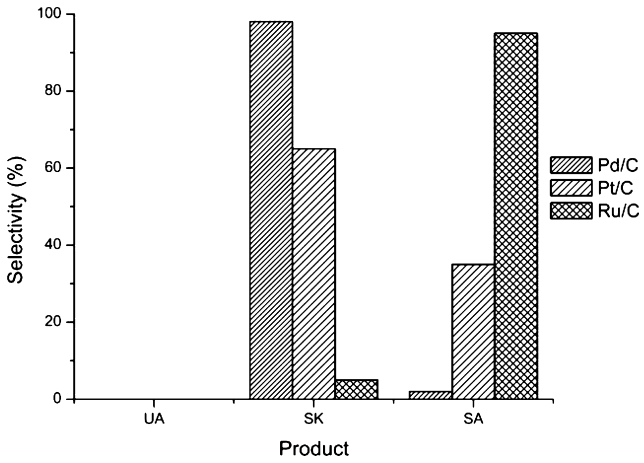

Figure 2. Selectivity during methyl vinyl ketone (MVK) hydrogenation after 3 h (complete conversion of MVK) over Pd/C, Pt/C, and Ru/C.

selectivity after 3 h (well after complete conversion of MVK) over Pd, Pt, and Ru. Although Ru/C and Pt/C readily converted the saturated ketone to the saturated alcohol, Pd/C was unable to effectively hydrogenate the carbonyl group.

The elementary steps involved in the sequential hydrogenation of the C═C and C═O bonds in MVK over the model Ru(0001) surface were investigated by carrying out DFT calculations. The hydrogenation of MVK was assumed to proceed from its most stable adsorption state on the Ru(0001) surface where MVK is oriented parallel to the surface in a planar η^4 configuration that allows both the C═C and C═O bonds to interact directly with four Ru atoms in the surface, as shown in Figure 3a. A similar η^4 adsorption mode was found in the adsorption of different unsaturated aldehydes (acrolein, crotonaldehyde, and prenal) on Pt(111).[41] The first hydrogen atom can add to the oxygen (O^1) or carbon (C^2) atoms of the C═O bond or to the secondary (C^3) or primary (C^4) carbon atoms of the C═C bond to form the IO, I2, I3, and I4 intermediates shown in Figure 4 via paths a1, a2, a3, and a4, respectively. All four of these partially hydrogenated alkoxy or alkyl intermediates shown in the center of Figure 4 bind to the Ru surface via the remaining unsaturated C or O atom in the activated C═C or C═O bond and the unaltered C═C or C═O bonds, thus resulting in the formation of η^3 adsorption structures. The adsorption energies for all four of these intermediates as well as the reactants and products (UA and SK) are reported in Table 3. The bond lengths for all of the structures examined are reported in the Supporting Information.

The DFT-calculated activation barriers for the addition of the first hydrogen to the C═C and C═O of adsorbed MVK reported in Figure 4 increase in the following order:

$$C^4 \text{ path a4} < C^2\text{–(O) path a2} < C^3\text{path a3} < O^1 \text{ path a1} \quad (1)$$

where C^4, C^2–(O), C^3, and O^1 refer to the addition of hydrogen to the terminal (primary) carbon atom of the C═C bond, the carbon of the C═O bond, the secondary carbon of the C═C bond, and the oxygen of the C═O bond on MVK, respectively. The asterisk in Figure 4 refers to an unsaturated carbon or oxygen that remains bonded to the metal surface after the initial hydrogenation step.

The ordering is largely dictated by the atom type (carbon or oxygen) and degree of substitution of the atom to which the hydrogen adds and the stabilization of the transition state that results from the creation of stronger Ru–O bond during alkoxide formation as compared with the weaker Ru–CHR bond that results from the formation of the hydroalkyl intermediate.

The activation barrier to add the first hydrogen to the primary (terminal) carbon atom of the C═C bond was calculated to be the lowest one of all four steps at 77 kJ mol^{-1} (path a4), since the addition of hydrogen to an sp^2 carbon atom is much more favored than the addition to an sp^2 oxygen atom and due to the fact that the primary carbon site has the fewest substituents in comparison with the other carbon sites and, thus, the lowest steric repulsion.

The barriers to hydrogenate at the secondary carbon center of the C═C (path a3) and the carbon of the C═O bonds (path a2) to form the I3 alkyl and I2 alkoxide intermediates are considerably higher than the barrier to add to the primary carbon (path a4) to form the I4 alkyl intermediate. This trend is the result of the higher degree of steric hindrance as well as the higher bond orders at the more substituted C centers, which decrease their stabilization by the surface in the transition state.

The barrier for the addition of hydrogen to the carbon of the carbonyl center (99 kJ mol^{-1}) is actually 10 kJ mol^{-1} lower than that for the addition to the secondary carbon center of the

dx.doi.org/10.1021/cs200567z | ACS Catal. 2012, 2, 671–683

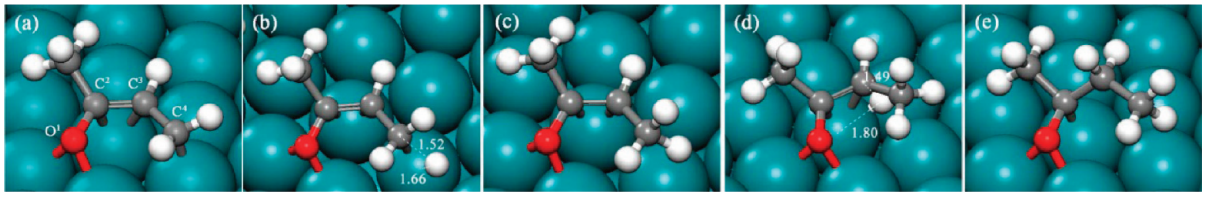

Figure 3. DFT-calculated structures during the hydrogenation of MVK to SK on Ru(0001), via pathways a4 and b4. (a) adsorbed MVK; (b) transition state (TS) of path a4; (c) intermediate I4; (d) transition state of path b4; (e) SK. Bond lengths are in angstoms.

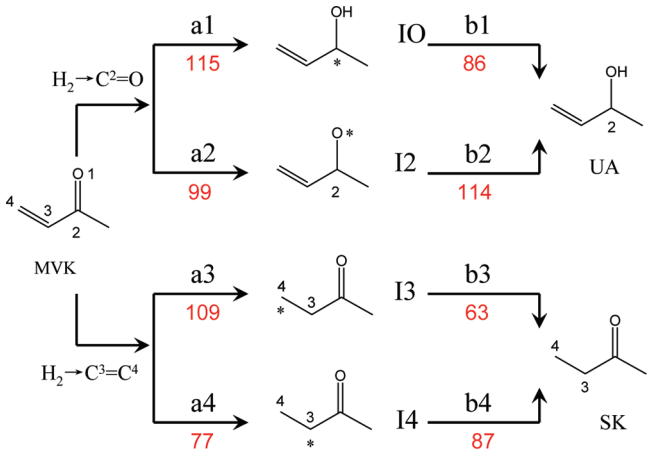

Figure 4. Scheme for the competitive hydrogenation routes of MVK. The first hydrogenation intermediates IO, I2, I3, and I4 are named after the hydrogen attack-centers. Pathways a1−a4 indicate the elementary reactions of the first hydrogenation step, and b1−b4 refer to the second hydrogenation reactions. Red numbers indicate the activation barriers (kJ mol^{-1}) occurring on Ru(0001). The asterisk refers to an unsaturated carbon or oxygen that remains bonded to the metal surface.

Table 3. Adsorption Energies (kJ mol^{-1}) for the Reactants (indicated by UK), Intermediates, and Products of MVK Hydrogenation on Ru(0001) and Benzalacetone Hydrogenation on Pt(111) and Ru(0001)

species	MVK Ru(0001)	benzalacetone Pt(111)	benzalacetone Ru(0001)
UK	−148	−100,[a] −17[b]	−272
IO	−177	−156	−374
I2	−300	−144	−335
I3	−195	−156	−297
I4	−178	−175	−305
UA	−113	−27	−228
SK	−28	−55	−122

[a]Adsorbed through aromatic ring and C═C. [b]Adsorbed through C═O.

C═C bond (109 kJ mol^{-1}). The higher degree of steric hindrance at the C^2 center over that at the C^3 center is overcome by the greater stabilization of the transition state as a result of the creation of a strong Ru−O bond in the transition state during the formation of the alkoxide intermediate over that of the Ru−CHR bond in the transition state during the formation of the alkyl intermediate. The difference is also reflected in the much stronger binding of the alkoxide intermediate (−300 kJ mol^{-1} for I2) over that of the alkyl intermediate (−195 kJ mol^{-1} for I3) that forms.

The highest initial activation barrier occurs for the addition of hydrogen to the O atom of the carbonyl (path a1), which has a barrier of 115 kJ mol^{-1}. This is the result of the intrinsic difference in forming the O−H bond versus the C−H bond on Ru and, in addition, to the weaker stabilization of the transition state by the surface to form the hydroxyalkyl compared with that of the alkoxide or the alkyl intermediates.

The addition of the second hydrogen atom to either the partially saturated C═O (Figure 4, steps b1 or b2) or C═C (Figure 4, steps b3 or b4) bonds produces the unsaturated alcohol (UA) or saturated ketone (SK). The barriers for each of these steps on Ru(0001) are shown on the right-hand side of Figure 4 and follow the same ordering as those presented for the first hydrogen addition step given in eq 1 above.

The addition of hydrogen to the primary alkyl intermediate via path b3 has the lowest barrier of all steps examined because of the favorable access of the primary carbon center that has very limited steric hindrance to hydrogen addition as well as to the fact that it has the lowest bond order. The addition of hydrogen to the alkoxide intermediate (I2) in path b2 was calculated to be the most difficult at 114 kJ mol^{-1}. This step requires the breaking of a very strong Ru−O bond, which is over 100 kJ mol^{-1} stronger than any of the other three alkyl intermediates. The barriers to hydrogenate the secondary hydroxyalkyl and alkyl intermediates shown in paths b1 and b4, respectively, both have modest barriers that fall between those for paths b2 and b3.

The potential energy surfaces for the four different paths involved in the hydrogenation of MVK to either UA or the SK are plotted together in Figure 5. The results indicate that the hydrogenation of the terminal C═C is significantly easier than the hydrogenation of the ketone. This can be explained by the lower steric hindrance and greater ease of hydrogenating the C═C bond, which consists of primary−secondary carbon centers over that of hydrogenating the unsaturated ketone, which consists of tertiary carbon and primary oxygen sites. In the absence of the excess steric hindrance at the carbonyl, there is a competition at the surface for the hydrogenation of the C═C vs C═O groups, as suggested previously by Loffreda in the hydrogenation of unsaturated aldehydes.[45]

These SK and UA products can either desorb from the surface or further hydrogenate to the saturated alcohol. The unsaturated alcohol binds much more strongly to the surface (−113 kJ mol^{-1}) than the saturated ketone (−28 kJ mol^{-1}). This is presumably the result of significant differences between the steric repulsion at the carbon center on the ketone versus that of the primary carbon center on the terminal olefin, as well as the difference between the bond strengths of the terminal OH and terminal CH_2 groups with Ru. The lower energy for desorption of the SK compared with the UA suggests that the UA would have a longer residence time on the surface during a catalytic reaction and would therefore be more likely to be further hydrogenated to the saturated alcohol (SA), which is consistent with the experimental results. In addition, once the C═C bonds of MVK are hydrogenated to the SK, significant amounts of the intermediate SK could be subsequently

dx.doi.org/10.1021/cs200567z | ACS Catal. 2012, 2, 671−683

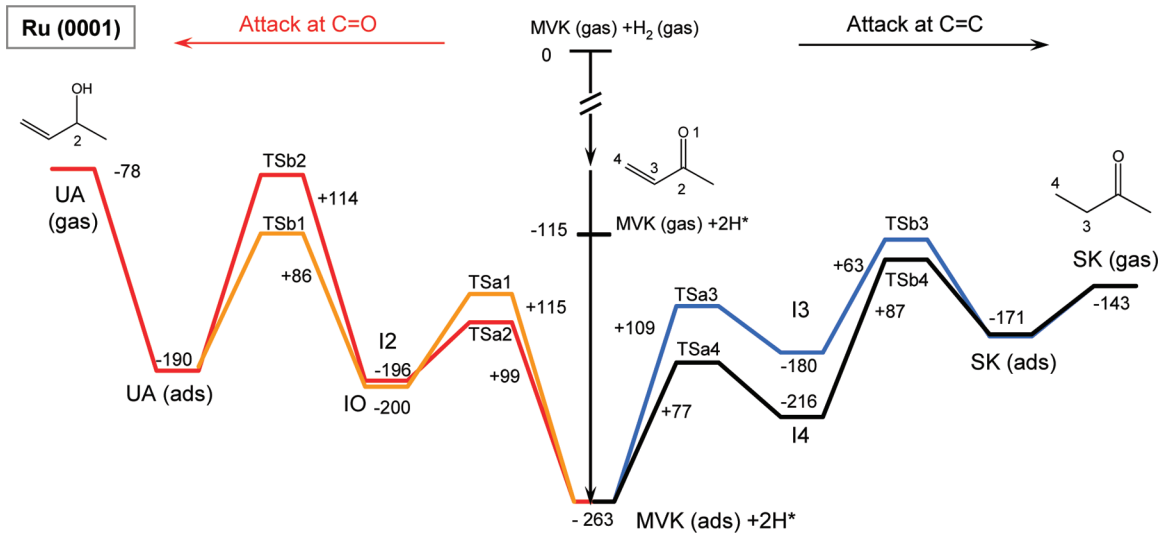

Figure 5. The energetic profiles for the partial hydrogenations of MVK on the Ru(0001) surface. "I-X" refers to the intermediates IO-I4. "TS" refers to transition states.

hydrogenated to the SA, as shown in Figure 2, because the activation barriers for C═O hydrogenation are not unreasonably high.

Although the hydrogenation of methyl vinyl ketone showed no appreciable selectivity toward the unsaturated alcohol over any of the carbon-supported metals investigated, some unsaturated alcohols were formed from crotonaldehyde hydrogenation over Pt, Ru, and Au. For example, the selectivity of crotonaldehyde hydrogenation (Table 2) over Pd/C was 100% to the saturated aldehyde, whereas some unsaturated alcohol was produced by Pt/C (S_{UA} = 10%) and Ru/C (S_{UA} = 17%). These results are consistent with those of Marinelli et al., who reported 13% selectivity to the unsaturated alcohol in the gas phase reaction over Pt/SiO_2.[10] Englisch et al. observed a selectivity of 11% to the unsaturated alcohol at 59% conversion of crotonaldehyde in methanol solvent and a selectivity of 20% to the unsaturated alcohol at 65% conversion of crotonaldehyde in ethanol solvent over a Pt/SiO_2 catalyst.[26] However, Riguetto et al. found that 100% saturated aldehyde was produced during hydrogenation of crotonaldehyde in the gas phase over Ru/SiO_2.[14]

Our results from hydrogenation of crotonaldehyde are generally consistent with those from MVK because hydrogenation of the C═C is the major product in both cases. The Pd/C catalyst was unable to effectively hydrogenate the C═O bond, and both Ru and Pt prefer to hydrogenate the C═C bond prior to hydrogenating the carbonyl group. The observation of unsaturated alcohol formed during crotonaldehyde hydrogenation over Pt, Ru, and Au compared with the complete lack of unsaturated alcohol formed during MVK hydrogenation over any of the metal catalysts illustrates the importance of substituent groups at the carbonyl and olefinic positions.

The TOF for hydrogenation over Pd/C was greater than that over Pt/C and Ru/C for both substrates (MVK and crotonaldehyde), and the Pt/C catalyst was slightly more active than the Ru/C catalyst. The Au/C catalyst, however, had a significantly lower TOF, which would be expected because of the low affinity of Au for dissociation of dihydrogen. For the Pd, Pt, and Ru catalysts, the TOF for MVK hydrogenation was significantly greater than that for crotonaldehyde, whereas the difference between the substrates was reduced on the Au catalyst. The high rate of C═C hydrogenation in MVK compared with crotonaldehyde over Pd/C (Table 2) was likely the result of the lower degree of substitution at the C═C bond of MVK over that of crotonaldehyde. The reduction of steric constraints in MVK compared with crotonaldehyde most likely results in a lower barrier to hydrogenate MVK. Since substitution near the C═C and C═O bonds appeared to affect both the selectivity and activity of the metal catalysts, more highly substituted substrates were also investigated at similar conditions.

Hydrogenation of Benzalacetone and Cinnamaldehyde. To examine the effect of steric influences at the C═C bond on the selectivity between the UA and the SK in the hydrogenation of unsaturated ketones and aldehydes, we examined the hydrogenation of benzalacetone (BA) and cinnamaldehyde, respectively, over supported Pd, Pt, Ru, and Au catalysts. Both BA and cinnamaldehyde have a phenyl group α to the C═C, which should decrease the rate of C═C hydrogenation and may potentially enhance the selectivity toward C═O hydrogenation over that of C═C hydrogenation.

Table 4 compares the results from the hydrogenation of BA and cinnamaldehyde over Pd/C, Pt/C, Ru/C, and Au/C in

Table 4. Hydrogenation of Benzalacetone and Cinnamaldehyde over Supported Pd, Pt, Ru, and Au Catalysts in Ethanol Solvent[a]

				selectivity (%)[b]		
substrate	catalyst	TOF[c] s^{-1}	conversion (%)[d]	UA	SK/SAL	SA
benzalacetone	Pd/C	9.4	69	0	96	4
benzalacetone	Pt/C	1.9	69	0	95	5
benzalacetone	Ru/C	1.2	64	0	95	5
benzalacetone	Au/C	0.016[e]	47	0	97	3
cinnamaldehyde	Pd/C	1.4	62	0	72	28
cinnamaldehyde	Pt/C	0.22	54	44	40	16
cinnamaldehyde	Ru/C	0.13	61	41	39	20
cinnamaldehyde	Au/C	0.011[e]	40	34	51	15

[a]Reaction conditions: 0.2 M substrate, $S/M_{surf} \sim 5000$, pH_2 = 2 atm, T = 333 K. [b]Selectivity is reported at the level of conversion in the table. [c]Turnover frequency is reported at ~20% conversion. [d]Conversion of benzalacetone or cinnamaldehyde. [e]Turnover frequency of Au/C reported at ~10% conversion.

dx.doi.org/10.1021/cs200567z | ACS Catal. 2012, 2, 671–683

ethanol. The hydrogenation of cinnamaldehyde to hydrocinnamaldehyde in ethanol produced a significant amount of byproduct, hydrocinnamaldehyde diethyl acetal. Hydrocinnamaldehyde diethyl acetal has been reported to always be in equilibrium with hydrocinnamaldehyde, and thus, the two are often reported together in reactivity studies.[22,25,31]

A high selectivity toward the saturated ketone during BA hydrogenation was observed over all of the carbon-supported catalysts. Milone et al. also reported 97.5% selectivity toward the saturated ketone at 36.3% conversion during liquid phase BA hydrogenation over Ru/Fe_2O_3.[11] For cinnamaldehyde hydrogenation, Ru/C, Pt/C, and Au/C produced significant amounts of the unsaturated alcohol, whereas Pd/C was completely unselective (see Table 4). These results are consistent with the findings reported earlier by Lashdef et al., who observed that a Pd/C catalyst was almost 100% selective toward the saturated aldehyde in liquid-phase cinnamaldehyde hydrogenation and Ru/C was about 30% selective toward unsaturated alcohol.[21] As summarized in Table 4, the carbon-supported Au catalyst produced slightly less unsaturated alcohol than the Ru and Pt catalysts.

The phenyl group is rather bulky and may sterically hinder hydrogenation at the C^4 site of the C═C bond. Despite the structural differences that result from substituting the methyl group on the vinyl ketone backbone of MVK with the bulkier phenyl group in BA, there was still no observed production of unsaturated alcohol over any of the carbon-supported metals. Thus, DFT calculations were carried out to examine the hydrogenation mechanisms and to draw comparisons with the results reported above for MVK hydrogenation. The calculations explored the hydrogenation of BA over both the model Pt(111) and Ru(0001) surfaces. Benzalacetone was found to adsorb on the Pt(111) surface either via its aromatic ring and C═C bond (Figure 6a-1) or only via its C═O bond (Figure S3b of the Supporting Information). The former configuration has a significantly stronger adsorption energy (−100 kJ mol^{-1}) than the latter one (−17 kJ mol^{-1}, Table 3) because it involves the adsorption of both the aromatic ring (∼−70 kJ mol^{-1}) and the C═C bond. Similar to BA, unsaturated aldehydes such as acrolein also interact with Pt(111), mainly via its C═C bond, but only a weak interaction with the oxygen atom was observed.[41] On Pt(111), we consider the hydrogenation of the C═C bond starting only from the adsorbed state (Figure 6a-1) and the hydrogenation of the C═O bond starting only from adsorption state (Figure S3b of the Supporting Information).

The binding energies for BA, the four partially hydrogenated intermediates (IO, I2, I3, I4), and the UA and SK products on Pt(111) and Ru(0001), are reported in Table 3. The optimized structures and bond lengths for each of these intermediates on both Pt(111) and Ru(0001) can be found in the Supporting Information. The results reveal that the adsorption energies for all of the species examined on Ru are considerably higher than those on Pt. The adsorption of BA, for example, was calculated to be −272 kJ mol^{-1} on Ru(0001), which is −172 kJ mol^{-1} stronger than that on Pt(111). The stronger adsorption on Ru over Pt is attributed to the stronger Ru−C and Ru−O bonds than the Pt−C and Pt−O bonds as well as the more favorable orientation of the phenyl, C═C, and C═O bonds on the Ru(0001) surface (Figure 6a-2) as compared with Pt(111). Similarly, the intermediates and products were bound much more strongly to Ru than to Pt, for example, IO (−374 kJ mol^{-1} on Ru versus −156 kJ mol^{-1} on Pt) and UA (−228 kJ mol^{-1} on Ru versus −27 kJ mol^{-1} on Pt). Analogous to the case with MVK, the unsaturated alcohol of BA was bound much more strongly to the Ru(0001) surface than the saturated ketone.

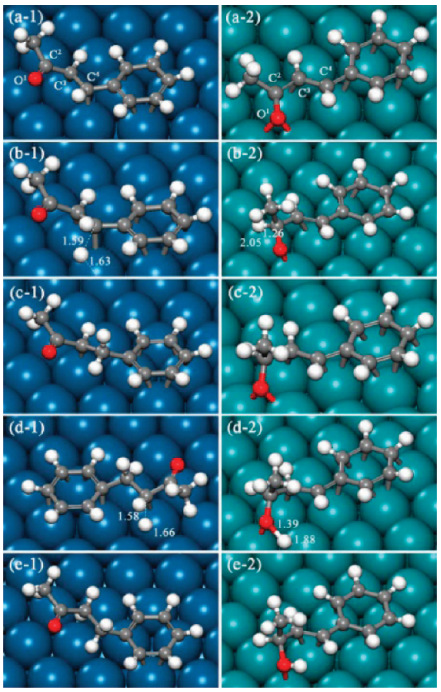

Figure 6. DFT-calculated structures during the hydrogenation of benzalacetone. Left-hand column: route that produces SK via intermediate I4 on Pt(111). (a-1) Adsorbed benzalacetone; (b-1) TS of path a4; (c-1) intermediate I4; (d-1) TS of path b4; (e-1) SK. Right-hand column: route producing UA via intermediate I2 on Ru(0001). (a-2) Adsorbed benzalacetone; (b-2) TS of path a2; (c-2) intermediate I2; (d-2) transition states of path b2; (e-2) UA. Bond lengths are in angstroms.

The calculated activation barriers and reaction energies for the hydrogenation of BA over Pt(111) for all four of the different reaction paths are shown in Figure 7 (energies depicted in blue) and in

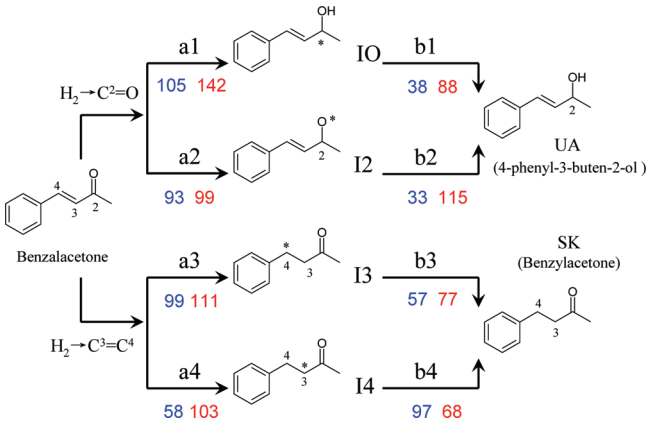

Figure 7. Scheme of competitive hydrogenation routes of benzalacetone. The first hydrogenation intermediates IO, I2, I3, and I4 are named after the hydrogen attack-centers. Pathways a1−a4 indicate the elementary reactions of the first hydrogenation step, and b1−b4 refer to the second hydrogenation reactions. Blue numbers indicate the activation barriers (kJ mol^{-1}) occurring on Pt(111); red numbers indicate the ones occurring on Ru(0001). The asterisk refers to an unsaturated carbon or oxygen that remains bonded to the metal surface after the initial hydrogenation step.

dx.doi.org/10.1021/cs200567z | ACS Catal. 2012, 2, 671−683

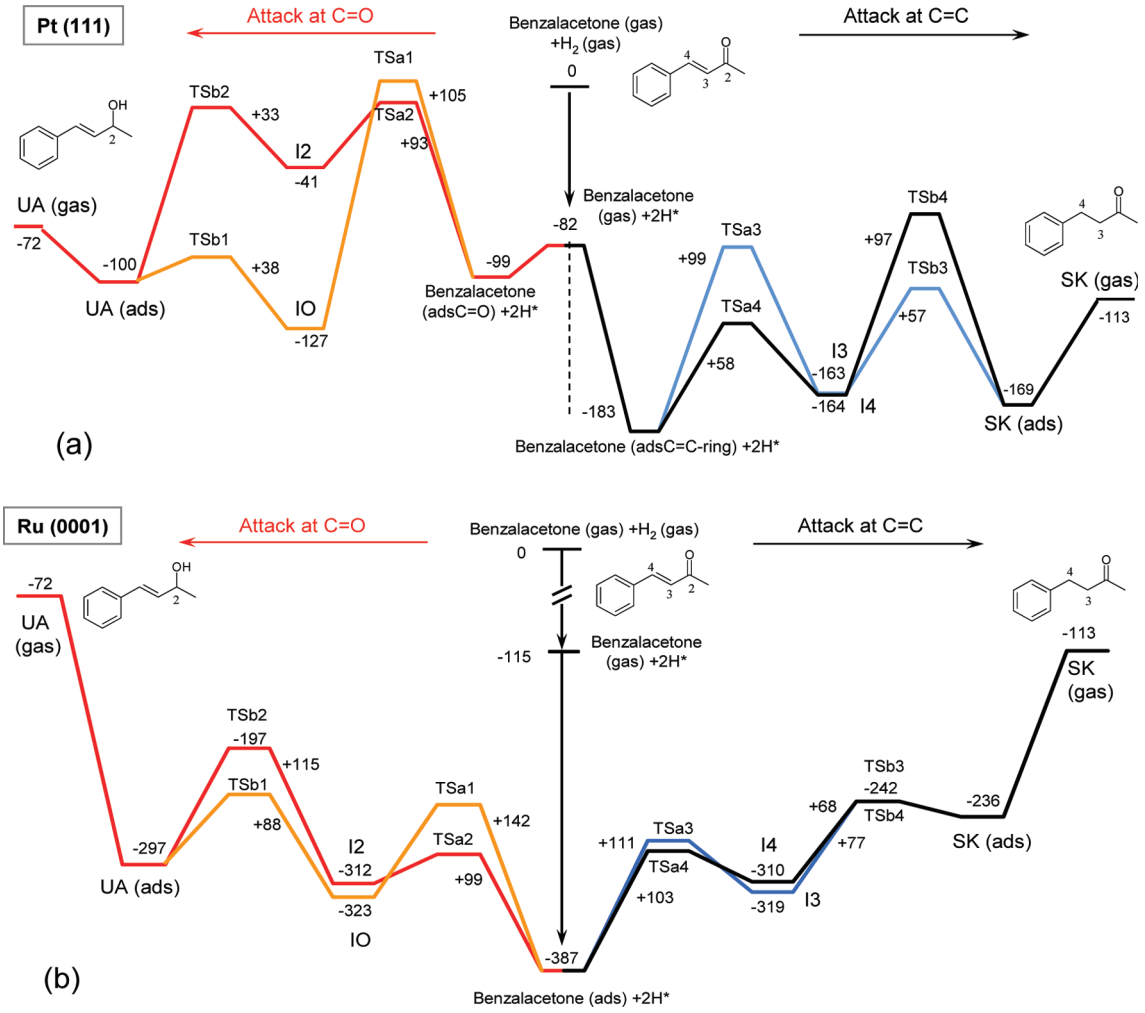

Figure 8. Potential energy profiles of the benzalacetone hydrogenation on (a) Pt(111) and (b) Ru(0001). Reaction energies and activation barriers are in kilojoules per mole.

Figure 8a. If the activation energies are measured with respect to the gas phase reactants, the barriers to hydrogenate the C═C bond are all considerably lower than those to hydrogenate the C═O bond. This trend can be seen by comparing the transition state energies (i.e., heights) of TSa1 and TSb2 to TSa3 and TSb4 in Figure 8a.

If the barriers, however, are measured with respect to the state of adsorbed BA and atomic hydrogen, they follow the same order as those presented in eq 1, above, for the hydrogenation of MVK over Pt(111):

$$C^4\text{–(phenyl) path a4} < C^2\text{–(O) path a2} < C^3\text{–(CH}_2\text{) path a3} < O^1 \text{ path a1} \quad (2)$$

and very similar order over Ru(0001):

$$C^2\text{–(O) path a2} < C^4\text{–(phenyl) path a4} < C^3\text{–(CH}_2\text{) path a3} < O^1 \text{ path a1} \quad (3)$$

The only difference between eq 3 and the results in eq 1 for MVK is the order of the C^2–(O) and C^4–(phenyl), which is caused by the introduction of the phenyl group at the C^4 position.

The lowest energy path for hydrogenating BA over Pt(111) proceeds by the addition of hydrogen to the carbon that is α to the aromatic ring via path a4, which has a barrier of only 58 kJ mol^{-1}. This path is significantly more favorable than the hydrogenation of the carbonyl bond, which proceeds via the addition of hydrogen to the C^2–(O) carbon center with a barrier of 93 kJ mol^{-1}. The structures for this path (a4–b4) are shown in Figure 6a-1–e-1. The barrier for the subsequent hydrogenation of the a4 alkyl intermediate to form the saturated ketone was calculated to be 97 kJ mol^{-1}. If we take into account the very weak adsorption of the carbonyl to the Pt(111) surface, the hydrogenation of C═O is clearly not favored, and UA is predicted to be a very minor product, which is consistent with the experimental results.

The rate of hydrogenation of the carbonyl over Pt(111) appears to be controlled by the initial addition of hydrogen to either the oxygen or the carbon of the carbonyl group, which have barriers of 105 and 93 kJ mol^{-1}, respectively. The subsequent hydrogenation of the I2 and IO intermediates were found to be only 33 and 38 kJ mol^{-1}.

The results over Ru(0001) are compared with those over Pt(111) in Figures 7 and 8. The results for Ru are shown in red in Figure 7 and in Figure 8b. The much stronger adsorption of the reactants and intermediates on Ru than those on Pt leads to higher intrinsic activation barriers for most of the hydrogen addition steps, which results in characteristic differences between the two metals. The initial hydrogenation of the C═C bond of adsorbed benzalacetone proceeds via the

dx.doi.org/10.1021/cs200567z | ACS Catal. 2012, 2, 671–683

addition of hydrogen to the carbon α to the phenyl group, which has a barrier of 103 kJ mol^{-1} on Ru that is significantly higher than that found on Pt (58 kJ mol^{-1}). The phenyl group is bound much more strongly to Ru(0001) than to Pt(111), which increases the steric repulsion at the C^4 site on Ru(0001), thus making it more difficult to add hydrogen to the C^4 position of the C=C bond. The very strong Ru−O interaction leads to a much stronger adsorption of alkoxide on Ru than on Pt, thus increasing the barrier of alkoxide hydrogenation (path b2, 115 kJ mol^{-1}) over that to actually form the alkoxide (path a2, 99 kJ mol^{-1}).

A closer analysis of C=O and C=C hydrogenation over Ru(0001) suggests that the initial hydrogen addition to the carbon of C=O via path a2 (with a barrier of 99 kJ mol^{-1}) is more favorable than the addition of hydrogen to the C^4 of the C=C bond via path a4 (103 kJ mol^{-1}). This can be attributed to the enhanced stabilization of the transition state that results from the formation of a strong Ru−O bond in the initial formation of the alkoxide intermediate over the weaker Ru-CHR bond in the formation of the alkyl intermediate. The difference is also reflected in the stronger binding of the alkoxide intermediate (−335 kJ mol^{-1} for I2) over that of the alkyl intermediate (−305 kJ mol^{-1}for I4) that forms. The activation barrier for the subsequent hydrogenation of the I2 alkoxy intermediate via path b2, however, is considerably higher (115 kJ mol^{-1}) than that for the subsequent hydrogenation of the I4 alkyl intermediate via path b4 (68 kJ mol^{-1}).

A comparison of the potential energy surfaces for both paths depicted in Figure 8b indicates that the I2 and I4 intermediates are likely quasi-equilibrated and as such, the apparent barriers can be taken from the adsorbed initial state and the transition state energies TSb2 (energy level −197 kJ mol^{-1}) and TSb4 (energy level −242 kJ mol^{-1}), which would result in an overall barrier of 190 kJ mol^{-1} (from the adsorbed reactant states) for route a2−b2 and 145 kJ mol^{-1} (from the adsorbed reactant states) for route a4−b4.

Alternatively, one can also reference the energies of TSb2 and TSb4 from the gas phase to show that similar trends in selectivity will be found, but with lower effective barriers. The results indicate that although the phenyl ring increases the barrier to hydrogenate the C=C bond in BA as compared with MVK, the C=C hydrogenation is still much more favorable than C=O hydrogenation, and the saturated ketone is still the major product that would be formed over supported Ru, which is consistent with the experimental results reported above.

Although the apparent barrier for the selective hydrogenation of BA to form the saturated ketone via the path a4-b4 is lower than that to form the unsaturated ketone via the path a1−b1, the difference is only 8 kJ mol^{-1}, which would suggest that some unsaturated alcohol might also be formed. The unsaturated alcohol, however, is strongly bound to the Ru surface, and on the basis of the calculated barrier, it should readily hydrogenate to the saturated alcohol before desorbing, which is consistent with the experimental results reported in Table 4, indicating that unsaturated alcohols are not observed over the various metals during BA hydrogenation.

In the hydrogenation of an α,β-unsaturated aldehyde, such as cinnamaldehyde, a high initial selectivity toward cinnamyl alcohol was observed over Pt/C and Ru/C and was maintained even at conversions greater than 50%. The carbonyl groups of BA and cinnamaldehyde were more readily hydrogenated on Pd/C than the carbonyl groups of either MVK or crotonaldehyde. However, Pd/C did not effectively catalyze the C=O bond of 2-butanone (saturated ketone of MVK). The substitution of a phenyl group for a methyl group on the C=C group of crotonaldehyde decreased the relative hydrogenation rate of the olefinic bond compared with that of the carbonyl.

The TOFs for both BA and cinnamaldehyde hydrogenation were greatest on the Pd catalyst (Table 4), as compared with Pt and Ru. Lashdaf et al. also reported that alumina and silica-supported Pd had a higher TOF for cinnamaldehyde hydrogenation than Ru.[20] Similar to the results in Table 2, the hydrogenation of C=C in the unsaturated ketone was faster than in the unsaturated aldehyde. A lower TOF for cinnamaldehyde versus BA hydrogenation over Au/Fe_2O_3 was attributed to acetal formation in the former case.[31] During cinnamaldehyde hydrogenation over Pd/C, significant amounts of acetal formation were observed at conversions greater than 10%, but the TOF did not change significantly from 2% to 35% conversion. Thus, we do not believe that acetal formation contributed to the significant differences in TOF between BA and cinnamaldehyde. Comparison of the turnover frequencies of the four probe molecules over Pd, Pt, and Ru catalysts (Table 2 and 4) suggests that the C=C hydrogenation of α,β-unsaturated ketones is faster than α,β-unsaturated aldehydes.

Although a direct quantitative comparison of MVK and BA hydrogenation is not possible because of the different solvents used in each experiment, we can use the results from theory carried out in the absence of solvent to understand qualitatively the differences between MVK and BA. As discussed previously, the adsorption of the reactants as well as all of the intermediates reported in Table 3 is stronger on Ru than on Pt as a result of the stronger Ru−C and Ru−O bonds than the Pt−C and Pt−O bonds. The stronger binding to Ru results in the higher calculated activation barriers for the hydrogenation of both the C=O and C−C bonds over Ru than Pt, which is consistent with the lower experimental TOF reported for the hydrogenation of MVK and BA over Ru than over Pt.

The DFT-calculated potential energy diagrams depicted in Figures 5 and 8 allow us to compare and analyze the hydrogenation of MVK and BA over Ru(0001). The results indicate that the substitution of the methyl group with a phenyl group α to the C^4 center on the C=C bond resulted in an increase of 26 kJ mol^{-1} in the barrier to add the first hydrogen to the C=C bond, since the barrier for the a4 path of MVK is only 77 kJ mol^{-1}, whereas that for BA is 103 kJ mol^{-1}. The strongly bound phenyl substituent sterically hinders the approach of the bound hydrogen in the transition state and significantly increases the adsorption strength of BA over MVK, both of which result in a higher C=C activation energy for BA over MVK. Although the intrinsic barrier for the hydrogenation of the C=C bond is significantly higher for BA than MVK, the apparent barrier for C=C hydrogenation of BA is still lower than that for C=O hydrogenation. The theoretical results presented in Figures 5 and 8 thus suggest that although the substitution of the phenyl group α to the C=C bond decreases the rate of hydrogenation, it does not influence the selectivity because the major product is still the saturated ketone. This is consistent with experimental results reported over Ru.

Influence of Support on Hydrogenation Reactions over Gold. As discussed earlier, Au/Fe_2O_3 has been reported to form some unsaturated alcohol from α,β-unsaturated ketone during hydrogenation reactions. As shown in Tables 2 and 4, Au/C was completely unselective for UA formation from unsaturated ketones under the conditions used in this study.

dx.doi.org/10.1021/cs200567z | ACS Catal. 2012, 2, 671−683

Table 5. Hydrogenation of MVK and Crotonaldehyde over Supported Au Catalysts in Aqueous Solvent[a]

substrate	catalyst	TOF[b] s^{-1}	conversion (%)[c]	selectivity (%)[d] UA	SK/SAL	SA
MVK	Au/C	0.019	26	0	95	5
MVK	Au/TiO_2	0.012	28	0	97	3
MVK	Au/Fe_2O_3	0.002	29	2	92	6
crotonaldehyde	Au/C	0.015	34	37	52	11
crotonaldehyde	Au/TiO_2	0.001	21	51	46	3
crotonaldehyde	Au/Fe_2O_3	0.001	26	40	47	13

[a]Reaction conditions: 0.2 M substrate, $S/M_{surf} \sim 5000$, $pH_2 = 2$ atm, $T = 333$ K. [b]Turnover frequency is reported at ~10% conversion. [c]Conversion of MVK or crotonaldehyde. [d]Selectivity is reported at the level of conversion in the table.

Table 6. Hydrogenation of MVK over Au/Fe_2O_3 at different S/M_{surf}[a]

substrate (mol)	catalyst (mol Au)	S/M_{surf}	TOF[c] s^{-1}	conversion (%)[d]	selectivity (%)[b] UA	SK/SAL	SA
6×10^{-4}	3×10^{-5}	19	0.001	41	19	75	6
5×10^{-3}	3×10^{-5}	159	0.001	36	8	89	3
6×10^{-4}	3×10^{-6}	180	0.002	32	5	88	7
5×10^{-3}	3×10^{-6}	5070	0.002	29	2	92	6

[a]Reaction conditions: 0.2 M substrate, $pH_2 = 2$ atm, $T = 333$ K. [b]Selectivity is reported at the level of conversion in the table. [c]Turnover frequency is reported at ~10% conversion. [d]Conversion of MVK.

Thus, the role of support on hydrogenation reactions catalyzed by Au particles was investigated.

Table 5 summarizes the results from hydrogenation of MVK and crotonaldehyde over Au/C, Au/TiO_2, and Au/Fe_2O_3. The TOF of all the gold catalysts was based on the time to reach 10% conversion. The low TOF of all gold catalysts compared with Pd, Pt, and Ru did not allow for high conversions to be achieved without significant errors in the carbon balance.

The hydrogenation of MVK over Au/Fe_2O_3 produced a small amount of unsaturated alcohol ($S_{UA} = 2\%$), whereas Au/C and Au/TiO_2 produced only the saturated ketone and traces of the saturated alcohol. Since the gold particle size on Au/TiO_2 and Au/Fe_2O_3 was similar, the different supports likely accounted for the small difference in selectivity during MVK hydrogenation to the unsaturated alcohol. The results of Milone et al. suggest that unique reactivity at the gold−goethite interface is the most likely reason for the selective hydrogenation of an α,β-unsaturated ketone to the unsaturated alcohol on Au/Fe_2O_3.[39] The selectivities during crotonaldehyde hydrogenation as reported in Table 5 revealed that all of the gold catalysts produced some of the unsaturated alcohol. This observation is consistent with the findings of Zanella et al., who investigated gas phase hydrogenation of crotonaldehyde over Au/TiO_2 prepared via deposition−precipitation with NaOH and urea.[35] As summarized in Table 5, the selectivity of the catalysts during crotonaldehyde hydrogenation ranged from 53 to 70%, whereas the TOF ranged from 0.0009 to 0.0078 s^{-1}. For crotonaldehyde hydrogenation, the Au/TiO_2 catalyst appeared to be more selective toward the unsaturated alcohol than Au/Fe_2O_3 and Au/C. The results in Table 5 indicate that Au-catalyzed hydrogenation of C═O in aldehydes was more effective than in ketones. In addition, supported Au catalysts were more selective to the unsaturated alcohol during crotonaldehyde hydrogenation than Pd, Pt, or Ru. However, the rate of hydrogenation over Au was also considerably slower than that over Pd, Pt, and Ru.

The effect of substrate-to-surface metal ratio on the reaction rate and product selectivity during MVK hydrogenation over Au/Fe_2O_3 was investigated, and the results are presented in Table 6. Although the reaction rate (TOF) remained relatively constant, the selectivity toward the unsaturated alcohol increased as the ratio of substrate to surface Au decreased (i.e., as more Au was added to the reactor). The largest selectivity of 19% to the unsaturated alcohol was observed at a high catalyst mass of 0.501 g with a low substrate concentration of 0.025 M. This result is similar to the 14% selectivity toward unsaturated alcohol reported by Milone et al. for 3-penten-2-one hydrogenation over Au/Fe_2O_3.[40] As given in Table 5, a reaction with a S/M_{surf} ratio of 159 had an unsaturated alcohol selectivity of 8%, and the S/M_{surf} ratio of 5070 had an unsaturated alcohol selectivity of 2%, although both runs utilized a 0.2 M solution of MVK. Thus, an increase in the amount of Au available contributed to an increase in the unsaturated alcohol selectivity for the Au/Fe_2O_3 catalyst.

Table 7 compares the hydrogenation of benzalacetone and cinnamaldehyde over the various Au catalysts. A high selectivity toward the unsaturated alcohol during benzalacetone hydrogenation over Au/Fe_2O_3 has been reported by Milone et al.[11,31,39,40] and is confirmed in this work. However, Au/C and Au/TiO_2 did not produce the unsaturated alcohol at the high substrate-to-metal ratio of 5000. The fact that unsaturated alcohol can be formed over Au/Fe_2O_3 during benzalacetone hydrogenation, whereas only trace amounts of unsaturated alcohol are formed over the same catalyst during MVK hydrogenation, is intriguing. The difference in selectivity could be attributed to the steric hindrance of the C═C bond by the phenyl group of benzalacetone. It is clear that particle size did not affect selectivity for benzalacetone, since Au/C has a much larger particle size than either Au/TiO_2 or Au/Fe_2O_3, but only Au/Fe_2O_3 had significant selectivity toward the unsaturated alcohol. Evidently, the iron oxide support contributed to an increased selectivity toward the formation of unsaturated alcohols from unsaturated ketones. However, for unsaturated aldehydes, Au/TiO_2 appeared to be a slightly more selective catalyst for the unsaturated alcohols. The rates of hydrogenation over the three gold catalysts were significantly lower than those over Pd, Pt, and Ru catalysts under identical

dx.doi.org/10.1021/cs200567z | ACS Catal. 2012, 2, 671−683

Table 7. Hydrogenation of Benzalacetone and Cinnamaldehyde over Supported Au Catalysts in Ethanol Solvent[a]

substrate	catalyst	TOF[b] s^{-1}	conversion (%)[c]	selectivity (%)[d]		
				UA	SK/SAL	SA
benzalacetone	Au/C	0.016	47	0	97	3
benzalacetone	Au/TiO_2	0.007	38	0	98	2
benzalacetone	Au/Fe_2O_3	0.001	45	38	47	15
cinnamaldehyde	Au/C	0.011	40	34	51	15
cinnamaldehyde	Au/TiO_2	0.004	42	52	39	9
cinnamaldehyde	Au/Fe_2O_3	0.001	49	46	40	14

[a]Reaction conditions: 0.2 M substrate, $S/M_{surf} \sim 5000$, $pH_2 = 2$ atm, $T = 333$ K. [b]Turnover frequency is reported at ~10% conversion. [c]Conversion of benzalacetone or cinnamaldehyde. [d]Selectivity is reported at the level of conversion in the table.

conditions, presumably because dihydrogen does not dissociate easily on pure gold surfaces.

CONCLUSIONS

The rate and selectivity for hydrogenation of methyl vinyl ketone, crotonaldehyde, benzalacetone (BA), and cinnamaldehyde with H_2 over supported metal catalysts Pd/C, Pt/C, Ru/C, Au/C, Au/TiO_2, and Au/Fe_2O_3 were compared under similar conditions. In general, the hydrogenation rate of α,β-unsaturated ketones was greater than that of α,β-unsaturated aldehydes over all catalysts under the conditions of 333 K and 1 atm H_2. However, the TOFs of all supported Au catalysts were significantly lower than those of Pd, Pt, and Ru. Although Au/TiO_2 was the most selective catalyst for producing unsaturated alcohols from unsaturated aldehydes, only Au/Fe_2O_3 was able to partially hydrogenate unsaturated ketones to unsaturated alcohols. Increasing the gold loading in the reactor relative to the amount of substrate increased the selectivity of MVK hydrogenation to the unsaturated alcohol.

The rate of hydrogenation over Pt and Ru was significantly slower than that over Pd, but Pt and Ru showed some selectivity to the unsaturated alcohol in the hydrogenation of α,β-unsaturated aldehydes. However, the carbonyl group of the ketones was hydrogenated on Pt and Ru only after nearly complete hydrogenation of the olefinic bond. Theoretical DFT calculations were carried out to examine the reactivity trends of MVK and benzalacetone during hydrogenation over model Pt(111) and Ru(0001) surfaces. Over the Ru surface, the hydrogenation of the terminal C═C bond of MVK is significantly easier than the hydrogenation of its ketone C═O bond. This is due to the considerably lower steric hindrance at the primary-secondary C═C versus the more sterically crowded C center of C═O and, in addition, the relative ease of hydrogenating the weaker $Ru\text{-}CH_2R$ bonds over the strong Ru-OR bonds. Both the primary reaction products, UA and SK, can either desorb from the surface or be further hydrogenated to form the saturated alcohol (SA), whereas the desorption of the more weakly held SK is easier compared with the UA. This is consistent with the experimental results that no UA and a small amount of SA (2%) are obtained in the hydrogenation of MVK over Ru/C at 72% conversion.

Theoretical calculations on benzalacetone (BA) hydrogenation were compared with those on MVK to elucidate the influence of steric inhibition at the C═C bond and electronic effects on the selectivities. The binding energies for the reactants as well as the intermediates of BA were found to be much stronger on the Ru surface than on Pt. Both primary products UA and SK were strongly bound to surface, which indicates a possibility of being further hydrogenated to saturated alcohol. However, desorption of the SK of benzalacetone was calculated to require much lower energy when compared with the UA over the Ru surface.

The calculated barriers for benzalacetone hydrogenation were found to be significantly higher over Ru compared with Pt, which is consistent with the lower experimental TOF reported over Ru than Pt. Over Pt, the addition of the first hydrogen to the C═O bond preferentially occurs at the C center with a barrier that is significantly higher than that to hydrogenate the C═C bond. Over the Ru surface, the presence of phenyl substituent of the C═C bond in benzalacetone increases the C═C hydrogenation barrier by 26 kJ mol^{-1} when compared with the methyl substituted C═C bond in MVK, but it does not change the relative C═C to C═O hydrogenation barriers enough to affect the selectivity trend. This is consistent with experimental results reported over Ru that showed the substitution of the phenyl group α to the C═C bond slows down the rate of C═C hydrogenation over all metals investigated.

ASSOCIATED CONTENT

Supporting Information

Supporting Information includes characteristic bond lengths, activation barriers, reaction energies, adsorption configurations, and the structures of transition states for DFT calculations. This material is available free of charge via the Internet at http://pubs.acs.org/.

AUTHOR INFORMATION

Corresponding Author

*E-mail: rjd4f@virginia.edu.

Notes

The authors declare no competing financial interest.

ACKNOWLEDGMENTS

This material is based upon work supported by the National Science Foundation under Award No. EEC-0813570 and through the EPSRC through CASTech. M.N. also acknowledges discussions with Chris Hardacre, Jillian M. Thompson, and Robbie Burch (Queens University) and Hugh Stitt (Johnson and Matthey). We also gratefully acknowledge the computational support from the Molecular Science Computing Facility (MSCF) in the William R. Wiley Environmental Molecular Sciences Laboratory, a national scientific user facility sponsored by the U.S. Department of Energy's Office of Biological and Environmental Research and located at the Pacific Northwest National Laboratory. Pacific Northwest is operated for the Department of Energy by Battelle.

REFERENCES

(1) Augustine, R. L. *Heterogeneous Catalysts in Organic Synthesis*; Dekker: New York, 1995.
(2) Mertens, P. G. N.; Vandezande, P.; Ye, X.; Poelman, H.; Vankelecom, I. F. J.; De Vos, D. E. *Appl. Catal., A* **2009**, *355*, 176.
(3) Gargano, M.; D'orazio, V.; Ravasio, N. *J. Mol. Catal.* **1990**, *58*, L5−L8.
(4) Coman, S. N.; Parvulescu, V. I.; De Bruyn, M.; De Vos, D. E.; Jacobs, P. A. *J. Catal.* **2002**, *206*, 218−229.
(5) Sharf, V.; Freidlin, L. *Russ. Chem. Bull.* **2008**, *21*, 1784−1785.
(6) Aramendia, M.; Borau, V.; Gomez, M.; Jimenez, C.; Marinas, J. *Appl. Catal.* **1983**, *8*, 177−185.
(7) Bond, G.C. *Catalysis of Metals*; Academic Press: London, 1962.
(8) Torres, G. C.; Ledesma, S. D.; Jablonski, E. L.; De Miguel, S. R.; Scelza, O. A. *Catal. Today* **1999**, *48*, 65−72.
(9) Von Arx, M. *J. Mol. Catal. A: Chem.* **1999**, *148*, 275−283.
(10) Marinelli, T.; Nabuurs, S.; Ponec, V. *J. Catal.* **1995**, *151*, 431−438.
(11) Milone, C.; Ingoglia, R. *Chem. Commun.* **2003**, *7*, 868−869.
(12) Margitfalvi, J.; Borbath, I.; Hegeds, M.; Tompos, A. *Appl. Catal., A* **2002**, *229*, 35−49.
(13) Mäki-Arvela, P.; Hájek, J.; Salmi, T.; Murzin, D. Y. *Appl. Catal., A* **2005**, *292*, 1−49.
(14) Steffan, M.; Lucas, M.; Brandner, A.; Wollny, M.; Oldenburg, N.; Claus, P. *Chem. Eng. Technol.* **2007**, *30*, 481−486.
(15) Lashdaf, M.; Krause, A.; Lindblad, M.; Tiitta, M.; Venalainen, T. *Appl. Catal., A* **2003**, *241*, 65−75.
(16) Lashdaf, M.; Hase, A.; Kauppinen, E.; Krause, A. O. I. *Science* **1998**, *52*, 199−204.
(17) Galvagno, S.; Capannelli, G.; Neri, G.; Donato, A.; Pietropaolo, R. *J. Mol. Catal.* **1991**, *64*, 237−246.
(18) Galvagno, S.; Milone, C.; Donate, A.; Neri, G.; Pietropaolo, R. *Catal. Lett.* **1993**, *18*, 349−355.
(19) Mercadante, L.; Neri, G.; Milone, C.; Donato, A.; Galvagno, S. *J. Mol. Catal. A: Chem.* **1996**, *105*, 93−102.
(20) Coq, B.; Kumbhar, P. S.; Moreau, C.; Moreau, P.; Warawdekar, M. G. *J. Mol. Catal.* **1993**, *85*, 215−228.
(21) Englisch, M.; Ranade, V.; Lercher, J. *Appl. Catal., A* **1997**, *163*, 111−122.
(22) Dandekar, A.; Vannice, M. A. *J. Catal.* **1999**, *183*, 344−354.
(23) Arai, M.; Obata, A.; Usui, K.; Shirai, M.; Nishiyama, Y. *Appl. Catal., A* **1996**, *146*, 381−389.
(24) Arai, M.; Usui, K.; Nishiyama, Y. *J. Chem. Soc. Chem. Comm.* **1993**, *24*, 1853−1854.
(25) Galvagno, S.; Donato, A.; Neri, G.; Pietropaolo, R. *Catal. Lett.* **1991**, *8*, 9−14.
(26) Riguetto, B. A.; Rodrigues, C. E. C.; Morales, M. A.; Baggio-Saitovitch, E.; Gengembre, L.; Payen, E.; Marques, C. M. P.; Bueno, J. M. C. *Appl. Catal., A* **2007**, *318*, 70−78.
(27) Špringerová, J.; Kacer, P.; Cerveny, L. *Res. Chem. Intermed.* **2005**, *31*, 785−795.
(28) Hammoudeh, A.; Mahmoud, S. *J. Mol. Catal. A: Chem.* **2003**, *203*, 231−239.
(29) Ponec, V. *Appl. Catal., A* **1997**, *149*, 27−48.
(30) Milone, C.; Crisafulli, C.; Ingoglia, R.; Schipilliti, L.; Galvagno, S. *Catal. Today* **2007**, *122*, 341−351.
(31) Milone, C.; Tropeano, M.; Gulino, G.; Neri, G. *Chem. Commun.* **2002**, *8*, 868−869.
(32) Milone, C.; Trapani, M. C.; Galvagno, S. *Appl. Catal., A* **2008**, *337*, 163−167.
(33) Schimpf, S.; Lucas, M.; Mohr, C.; Rodemerck, U.; Bruckner, A.; Radnik, J.; Hofmeister, H.; Claus, P. *Catal. Today* **2002**, *72*, 63−78.
(34) Zanella, R.; Louis, C.; Giorgio, S.; Touroude, R. *J. Catal.* **2004**, *223*, 328−339.
(35) Mohr, C.; Hofmeister, H.; Lucas, M.; Claus, P. *Chem. Eng. Technol.* **2000**, *23*, 324−328.
(36) Claus, P.; Brückner, A.; Mohr, C.; Hofmeister, H. *J. Am. Chem. Soc.* **2000**, *122*, 11430−11439.
(37) Mohr, C.; Hofmeister, H.; Radnik, J.; Claus, P. *J. Am. Chem. Soc.* **2003**, *125*, 1905−1911.
(38) Shibata, M.; Kawata, N.; Masumoto, T.; Kimura, H. *J. Chem. Soc., Chem. Comm.* **1988**, *3*, 154.
(39) Milone, C.; Ingoglia, R.; Schipilliti, L.; Crisafulli, C.; Neri, G.; Galvagno, S. *J. Catal.* **2005**, *236*, 80−90.
(40) Milone, C.; Ingoglia, R.; Pistone, A.; Neri, G. *J. Catal.* **2004**, *222*, 248−356.
(41) Delbecq, F.; Sautet, P. *J. Catal.* **2002**, *211*, 398−406.
(42) Loffreda, D.; Delbecq, F.; Sautet, P. *Chem. Phys. Lett.* **2005**, *405*, 434−439.
(43) Hirschl, R.; Delbecq, F.; Sautet, P.; Hafner, J. *J. Catal.* **2003**, *217*, 354−366.
(44) Kang, G.; Chen, Z.; Li, Z. *Catal. Lett.* **2011**, *141*, 996−1003.
(45) Loffreda, D.; Delbecq, F.; Vigne, F.; Sautet, P. *Angew. Chem., Int. Ed.* **2005**, *44*, 5279−5282.
(46) Lim, K. H.; Mohammad, A. B.; Yudanov, I. V.; Neyman, K. M.; Bron, M.; Claus, P.; Rosch, N. *J. Phys. Chem. C* **2009**, *113*, 13231−13240.
(47) Hirschl, R.; Eichler, A.; Hafner, J. *J. Catal.* **2004**, *226*, 273−282.
(48) Hirschl, R.; Delbecq, F.; Sautet, P.; Hafner, J. *Phys. Rev. B* **2002**, *66*, 155438−155449.
(49) Khanra, B. C.; Jugnet, Y.; Bertolini, J. C. *J. Mol. Catal., A* **2004**, *208*, 167−174.
(50) Loffreda, D.; Delbecq, F.; Vigne, F.; Sautet, P. J. *J. Am. Chem. Soc.* **2006**, *128*, 1316−1323.
(51) Laref, S.; Delbcq, F.; Loffreda, D. *J. Catal.* **2009**, *265*, 35−42.
(52) Kliewer, C. J.; Bieri, M.; Somorjai, G. A. *J. Am. Chem. Soc.* **2009**, *131*, 9958−9966.
(53) Hohenberg, P.; Kohn, W. *Phys. Rev.* **1964**, *136*, B864−B871.
(54) Kresse, G.; Furthmuller, J. *Phys. Rev. B* **1996**, *54*, 11169−11186.
(55) Perdew, J. P.; Chevary, J.; Vosko, S.; Jackson, K. A.; Pederson, M. R.; Singh, D.; Fiolhais, C. *Phys. Rev. B* **1992**, *46*, 6671−6687.
(56) Vanderbilt, D. *Phys. Rev. B* **1985**, *32*, 8412−8415.
(57) Monkhorst, H. J.; Pack, J. D. *Phys. Rev. B* **1976**, *13*, 5188−5192.
(58) Methfessel, M.; Paxton, A. *Phys. Rev. B* **1989**, *40*, 3616−3621.
(59) Ashcroft, N.W.; Mermin, N.D. *Solid State Physics*; Holt, Rinehart and Winston: New York, 1976.
(60) Landolt-Börnstein, N. *Structure Data of Elements and Intermetallic Phases*: Springer-Verlag: Berlin, 1971.
(61) Henkelman, G. *J. Chem. Phys.* **2000**, *107*, 10229.
(62) Sheppard, D.; Terrell, R.; Henkelman, G. *J. Chem. Phys.* **2008**, *128*, 134106.
(63) Henkelman, G. *J. Chem. Phys.* **1999**, *81*, 168.
(64) Heyden, A.; Bell, A. T.; Keil, F. J. *J. Chem. Phys.* **2005**, *123*, 224101.
(65) Neurock, M.; Pallassana, V.; Van Santen, R. A. *J. Am. Chem. Soc.* **2000**, *122*, 1150−1153.
(66) Akpa, B. S.; D'Agostino, C.; Gladden, L. F.; Hindle, K.; Manyar, H.; McGregor, J.; Li, R.; Neurock, M.; Sinha, N.; Stitt, E. H.; Weber, D.; Zeitler, J. A.; Rooney, D. W. *J. Catal.* **2012**, doi: 10.1016/j.jcat.2012.01.011.
(67) Sinha, N., Ph.D. Dissertation, University of Virginia, May 2009.